Effects of nanoparticle geometry on photon statistics

Luke C. Ugwuoke[1], **Tjaart P. J. Krüger**[1], **and Mark S. Tame**[2]

[1] Department of Physics, University of Pretoria, Private Bag X20, Hatfield 0028, South Africa
[2] Department of Physics, Stellenbosch University, Private Bag X1, Matieland 7602, South Africa

E-mail: lcugwuoke@gmail.com

Abstract. A quantum study of the geometry-dependent light scattering by a metamolecule weakly driven by a plane-polarized electric field is presented. The metamolecule consists of a semiconductor quantum dot coupled to a silver nanoparticle. We show that a transition from bunching to antibunching of the scattered photons by the metamolecule varies with the quantum dot–nanoparticle distance as the nanoparticle geometry is tuned from prolate to oblate to spheric at constant particle volume. We attribute this to the geometry-dependent quantum dot–nanoparticle coupling, localized surface plasmon resonance, and dipole moment of the nanoparticle.

1. Introduction

Metal nanoparticle (MNP)–quantum dot (QD) systems are capable of emitting non-classical light when they interact with the coherent light from a laser source [1–4]. These systems, also referred to as metamolecules [4], have been proposed for various quantum control applications [1, 3]. Furthermore, non-classical light can be used for carrying out quantum communication [5] and refractive index sensing [6].

The QD is usually a photostable, semiconducting emitter, such as cadmium selenide (CdSe), with tunable ground-state, exciton transition frequency, ω_{ex}, and spontaneous decay rate, γ_{ex} [7], often modelled as a two-level atom, as shown in Fig. 1(a). Previous studies have considered the interaction between the localized surface plasmon resonance (LSPR) of a spherical MNP and the QD exciton [1–4]. The interaction between the narrow-linewidth exciton and the broad-linewidth LSPR leads to the appearance of a scattering spectrum with a Fano profile — an asymmetric lineshape with both constructive (Fano peak) and destructive (Fano dip) interference regions [1, 2, 7].

Ridolfo et al. [1] have previously shown that the driven metamolecule can exhibit photon antibunching — a quantum effect where a driven scatterer emits photons with a near-regular photocount pattern during absorption–spontaneous emission events [8,9] — in the weak-driving limit. According to Waks et al. [2], this is the limit where the modified Rabi frequency of the QD, Ω, is small compared to the enhanced QD decay rate, Γ, as well as where the semiclassical approximation is valid. In this study, we investigated the photon statistics of both spherical- and spheroidal-based metamolecules. In the latter, the QD exciton interacts with the longitudinal LSPR of the spheroids, as shown in Fig. 1(b). The spherical-based metamolecule is a special case of spheroidal-based metamolecules, whose photon statistics were studied here to ensure that our model is in good agreement with Refs. [1, 2, 4]. In addition, we also investigated the dependence of the photon statistics on the MNP-QD distance.

2. Theory

The approach proposed in Ref. [1] is used here to obtain the second-order correlation function for zero-time delay, $g^{(2)}(0)$ — a statistical parameter that determines whether the scattered photons will arrive

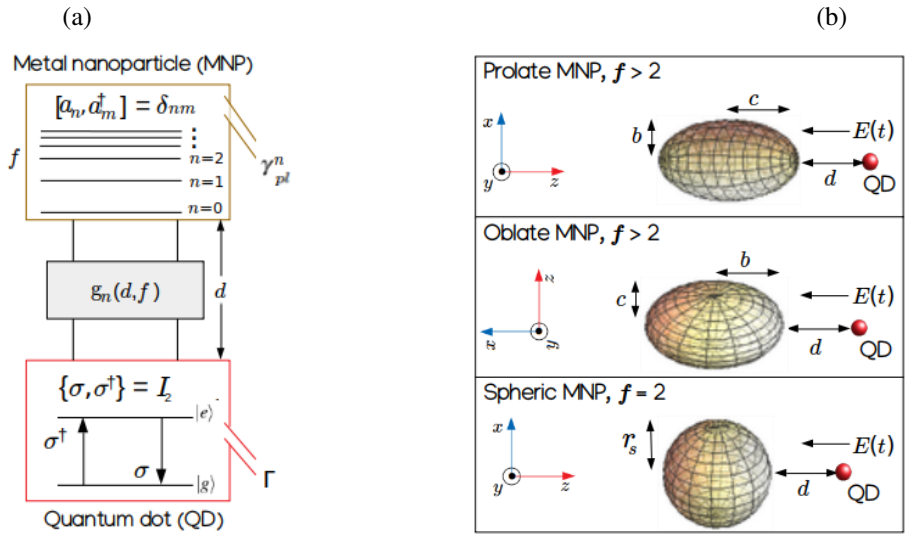

Figure 1. (a) Quantum electrodynamics (QED) model of the metamolecule. The MNP has a geometric factor f, and plasmon modes with angular momentum numbers $n = 0, 1, 2, ...$, corresponding to the plasmon resonances $0, \omega_{pl}^1, \omega_{pl}^2, ...$, with non-radiative decay rates $0, \gamma_{pl}^1, \gamma_{pl}^2, ...$, respectively. The MNP is coupled to the QD through the coupling rate, g_n, which depends on both d and f, where d is the MNP-QD surface-to-surface distance. The QD is modelled as a two-level atom (with ground state $|g\rangle$ and excited state $|e\rangle$), which undergoes a decay rate enhancement, Γ, upon interaction with the MNP. The MNP operators, a and $a^\dagger$, obey the commutation rule, $[a_n, a_m^\dagger] = \delta_{nm}$, while the QD operators, σ and $\sigma^\dagger$, obey the anti-commutation rule, $\{\sigma, \sigma^\dagger\} = I_2$. (b) Model geometries of the metamolecule. The incident electric field, $E(t)$, is plane-polarized. We assume that the QD dipole couples longitudinally to the MNP dipole, where their dipole orientations lead to maximum effect. Each MNP is modelled as a Drude metal with a frequency-dependent dielectric function, $\varepsilon(\omega)$. The prolate has semi-axes $b \times b \times c, c > b$, the oblate has semi-axes $b \times b \times c, b > c$, and the spheric MNP has an equivalent sphere-volume radius, $r_s = \sqrt[3]{cb^2}$, so that while the MNP geometry is tuned through f, its volume remains constant.

randomly (for coherent light), regularly (for antibunched light), or in bunches (for bunched light), at a detector [9].

In plasmonic cavity QED, the weak-coupling condition, $g < \gamma_{pl}$, required for the observation of photon antibunching is easily attainable [1, 3] due to the large value of γ_{pl}. Here, g is the dipole-dipole coupling rate between the QD and the MNP, and γ_{pl} is the decay rate of the plasmon dipole mode. Hence, we will determine $g^{(2)}(0)$ in the weak-coupling regime where the rotating-wave approximation is valid.

Finally, only the plasmon dipole mode $(n = 1)$ in Fig. 1(a) will be considered here. The plasmon multipolar modes $(n \geq 2)$ are dark modes which do not couple to the driving field but couple to the dipole mode. The validity of the dipole approximation has been investigated in Ref. [3], where it was shown that multipolar contributions are not negligible at short MNP-QD distances. However, in Ref. [1], it was shown that the dipole approximation is valid in the distance regime $d \geq r_{QD} + 2$ nm, where r_{QD} is the QD radius. Our study will keep to this latter regime.

The driving field of the laser is modelled as a cosine wave: $E(t) = E_0 \cos \omega t$, with amplitude, E_0, and driving frequency, ω. In the rotating-frame, the total Hamiltonian of the driven metamolecule is [1, 4]:

$$\mathscr{H} = \hbar\Delta_{pl} a^\dagger a + \hbar\Delta_{ex} \sigma^\dagger \sigma - E_0 \mu(\sigma + \sigma^\dagger) - E_0(\chi^* a + \chi a^\dagger) + i\hbar g(\sigma a^\dagger - \sigma^\dagger a), \tag{1}$$

where $\Delta_{pl} = \omega_{pl} - \omega$ and $\Delta_{ex} = \omega_{ex} - \omega$ are the plasmon-laser detuning and exciton-laser detuning

frequencies, respectively, $\omega_{ex} = \omega_{pl} - \delta$, δ is the exciton-plasmon detuning, and

$$\omega_{pl} \approx \sqrt{\frac{\omega_p^2}{\varepsilon_\infty + f\varepsilon_b} - \gamma_p^2}, \;\; \gamma_{pl} \approx \gamma_p + \frac{\gamma_p^3}{\omega_{pl}^2}, \tag{2a}$$

$$\chi \approx -ib(f+1)\varepsilon_b\sqrt{2\pi\hbar\varepsilon_0 c\eta(1-L)}, \;\; g \approx \frac{b\mu(f+1)}{(c+d)^3}\sqrt{\frac{c\eta[1-L(v)]}{2\pi\hbar\varepsilon_0}}, \tag{2b}$$

where ω_{pl} and χ are the dipolar LSPR and dipole moment of the MNP, respectively, $\mu = er_{QD}$ is the dipole moment of the QD, e is the electronic charge, $\hbar$ is Dirac's constant, ε_0 is the permittivity of free space, ε_b is the dielectric constant of the background medium, and ε_∞ is the high-frequency dielectric constant of silver, where we have ignored radiative damping since we are in the Rayleigh regime [1, 10]. In Eq. 2a, ω_p and γ_p are the Drude model parameters for the plasma frequency and free-electron damping rate of silver, respectively, $f = (1-L)/L$, where L is the static geometric factor of the free MNP as given in Ref. [10]. In Eq. 2b, $c \to c, b \to b$ (prolate), $c \to b, b \to c$ (oblate), $c \to r_s, b \to r_s$ (sphere), $\eta = \omega_p^2/[2\omega_{pl}(\varepsilon_\infty + f\varepsilon_b)^2]$, and $L = L(v) = 1/3$ for a sphere. For the spheroids, $L(v)$ is the static geometric factor of the MNP-QD system, with a radial coordinate, v, which we reported previously in Ref. [10].

The equation of motion describing the evolution of the expectation values of the MNP and QD operators, a and $a^\dagger$, and σ and $\sigma^\dagger$, respectively, in the Heisenberg picture, is given by [3]:

$$\frac{d\langle\mathscr{O}\rangle}{dt} = \frac{i}{\hbar}\langle[\mathscr{H},\mathscr{O}]\rangle + \frac{\gamma_{pl}}{2}\left(a^\dagger[\mathscr{O},a] + [a^\dagger,\mathscr{O}]a\right) + \frac{\gamma_{ex}}{2}\left(\sigma^\dagger[\mathscr{O},\sigma] + [\sigma^\dagger,\mathscr{O}]\sigma\right), \tag{3}$$

from which we obtain the following coupled equations in the weak-driving limit:

$$\frac{d\langle a\rangle}{dt} = -\left(i\Delta_{pl} + \frac{1}{2}\gamma_{pl}\right)\langle a\rangle + g\langle\sigma\rangle + i\Omega_{pl}, \tag{4a}$$

$$\frac{d\langle\sigma\rangle}{dt} = -\left(i\Delta + \frac{1}{2}\Gamma\right)\langle\sigma\rangle + i\Omega\left(1 - 2\langle\sigma^\dagger\sigma\rangle\right), \tag{4b}$$

$$\frac{d\langle\sigma^\dagger\sigma\rangle}{dt} = -\Gamma\langle\sigma^\dagger\sigma\rangle + i\left(\Omega\langle\sigma^\dagger\rangle - \Omega^*\langle\sigma\rangle\right), \tag{4c}$$

where we have applied the adiabatic approximation [2] (since $\gamma_{pl} >> \gamma_{ex}$) to obtain Eqs. 4b and 4c. The coupled equations are solved at steady-state conditions to obtain the coherences $\langle a\rangle, \langle\sigma\rangle$, the excited state population of the QD $\langle\sigma^\dagger\sigma\rangle$, as well as the modified QD parameters $\Omega = \Omega_{ex}(1 - (\chi/\mu)\sqrt{\mathscr{F}})$ (near-field enhancement), $\Gamma = \gamma_{ex} + \mathscr{F}\gamma_{pl}$ (Purcell effect), $\Delta = \Delta_{ex} - \mathscr{F}\Delta_{pl}$ (exciton shift), where $\mathscr{F} = 4g^2/(\gamma_{pl}^2 + 4\Delta_{pl}^2)$ is the plasmon-induced enhancement factor, $\Omega_{pl} = E_0\chi/\hbar$ is the driving frequency of the MNP, and $\Omega_{ex} = \mu E_0/\hbar$ is the Rabi frequency.

3. Results and Discussion

In the quantum picture, the dipole moments of the MNP and the QD are defined in terms of the expectation values of their respective operators, as [4] $\chi\langle a\rangle$ and $\mu\langle\sigma\rangle$, respectively, and the total dipole moment operator is $\mathscr{P}^+ = \chi a + \mu\sigma$. At steady-state, $g^{(2)}(0) = \langle(\mathscr{P}^-)^2(\mathscr{P}^+)^2\rangle/\langle\mathscr{P}^-\mathscr{P}^+\rangle^2$, and the scattering cross-section is proportional to $\langle\mathscr{P}^-\mathscr{P}^+\rangle$, where $\mathscr{P}^- = (\mathscr{P}^+)^\dagger$ [1, 3].

We have made use of the following model parameters of a CdSe QD and that of a silver nanoparticle from Ref. [1]: $r_{QD} = 0.7$ nm, $\gamma_{ex} = 50$ μeV, $\gamma_p = 53.26$ meV, $\delta = 60$ meV, $\varepsilon_b = 3.0, \varepsilon_\infty = 3.699$. The Rabi energy, $\mu E_0 = 0.01$ meV, ensures that we are in the weak-driving limit: $\Omega << \Gamma$. The MNP sizes we considered are $c = 13$ nm, $b = 12$ nm (prolate), $c = 12$ nm, $b = 13$ nm (oblate), and $r_s \approx 12.32$ nm (spheric). The semi-axes of the spheroids are chosen such that: $(f_{spheroid} - f_{sphere}) < \frac{1}{8}f_{sphere}$. This ensures that the respective aspect ratios of the spheroids are very close to that of the sphere, i.e, unity. Some of our analytical results have been verified using the quantum simulation toolbox QuTiP [11].

The scattering cross-section of the metamolecule gradually decreases as the MNP geometry is tuned from $f = 2.2$ (prolate) to $f = 2.0$ (spheric), as can be observed from the trend in the scattering peaks in Fig. 2(a). In addition, the wavelengths corresponding to the scattering peaks — the Fano peaks (peaks of the narrow and asymmetric lineshapes in Fig. 2(a)) and the plasmon peaks (peaks of the broad and symmetric lineshapes in Fig. 2(a)) — undergo blueshifts as the MNP geometry is tuned from prolate to spheric, as summarized in Table 1. This shows that each driven metamolecule is a good scatterer depending on the energy region in Fig. 2(a). At far distances, $d = 10$ nm, the scattering spectra of the metamolecule (broken coloured curves in Fig. 2(a)) approach those of the spectra of the free MNP (broken black curves in Fig. 2(a)), due to huge decreases in the coupling rates.

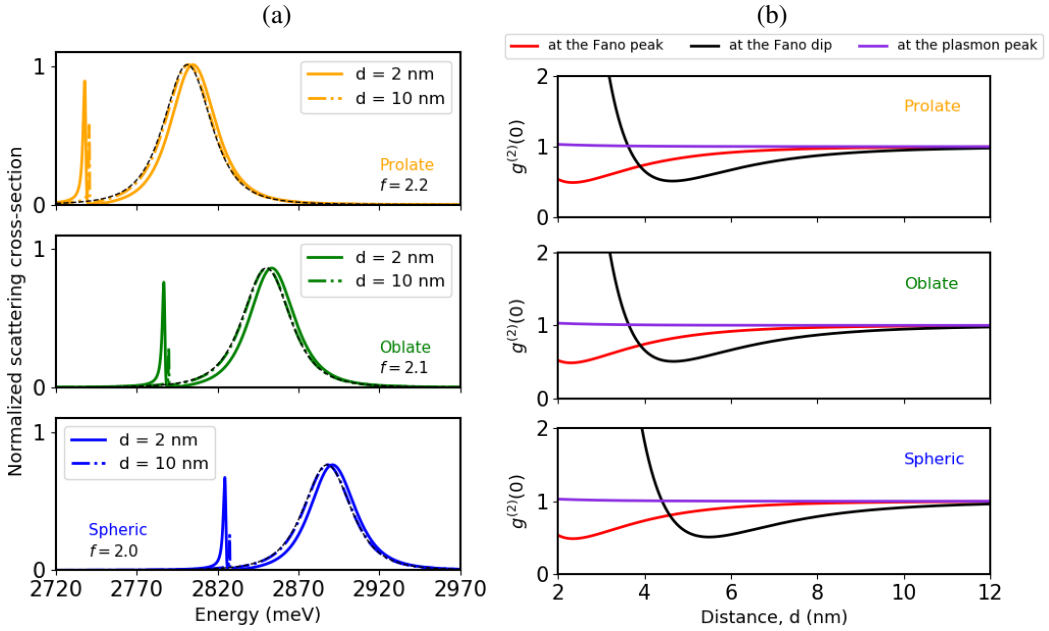

Figure 2. (a) Dependence of the scattering cross-section on the geometric factor, f, and on the MNP-QD distance, d. (b) Second-order correlation function for zero-time delay, $g^{(2)}(0)$, as a function of the MNP-QD distance, d.

Table 1. The Fano peak (Fano resonance), the Fano dip (transparency dip), and the plasmon peak (∼plasmon resonance) formed in the scattering spectrum of the metamolecule for each of the MNP geometries at $d = 2$ nm. (Deduced from Fig. 2(a).)

	ω (meV)		
Metamolecule	Fano peak	Fano dip	Plasmon peak
Prolate-based	~ 2737.77	~ 2739.66	~ 2805.31
Oblate-based	~ 2786.65	~ 2788.54	~ 2853.96
Spheric-based	~ 2824.44	~ 2826.56	~ 2891.27

Fano interference is responsible for the Fano dips in the scattering spectra in Fig. 2(a), as well as the resonances, $\omega'_{ex} \approx \omega_{ex} - \mathscr{F}\omega_{pl}$ (Fano resonance) and $\omega'_{pl} \approx \omega_{pl} + [g^2/(\omega_{pl} - \omega_{ex})]$ (plasmon resonance). The Fano dips are regions in-between the Fano peaks and the plasmon peaks where the metamolecule is transparent to the driving frequency, i.e, frequencies where $\langle \mathscr{P}^- \mathscr{P}^+ \rangle \to 0$. The interference effect weakens at long distances (such as at $d = 10$ nm in Fig. 2(a)), leading to: $\omega'_{ex} \to \omega_{ex}$ and $\omega'_{pl} \to \omega_{pl}$ since $g \to 0$. These resonances and the Fano dips are presented in Table 1 as driving frequencies, ω, where the metamolecule exhibits different photon statistics as shown in Fig. 2(b).

When driven at the plasmon peak, the metamolecule emits only coherent light ($g^{(2)}(0) = 1$), regardless of the distance, d, and the MNP geometry (Fig. 2(b), blue-violet curves). This is because, driving the metamolecule at the plasmon peak causes elastic scattering by the MNP to dominate the photon statistics. Hence, the square of one-photon scattering probability, $\langle \mathscr{P}^- \mathscr{P}^+ \rangle^2$, is the same as the two-photon scattering probability, $\langle (\mathscr{P}^-)^2 (\mathscr{P}^+)^2 \rangle$.

At the Fano dip, the scattered photons are heavily bunched ($g^{(2)}(0) > 1$) at short distances, $d \leq 4$ nm, and antibunched ($g^{(2)}(0) < 1$) at 4 nm $< d \leq 8$ nm, but coherent scattering ($g^{(2)}(0) \to 1$) dominates at long distances, $d > 8$ nm (Fig. 2(b), black curves). Though the scattering of an incident photon is suppressed at the Fano dip due to destructive interference, a pair of simultaneous incident photons will saturate the metamolecule's ground state transition, thereby increasing the two-photon scattering probability, $\langle (\mathscr{P}^-)^2 (\mathscr{P}^+)^2 \rangle$. Thus, at short distances, driving at the Fano dip leads to a bunching effect because the metamolecule acts as a saturable scatterer. The transition from bunched to antibunched light between $d > 4$ nm and $d = 8$ nm is due to a frequency shift, i.e, the Fano dip at $d = 2$ nm is a Fano peak between $d > 4$ nm and $d = 8$ nm. At $d > 8$ nm, the Fano effect disappears and the response returns to that of the MNP, which gives coherent scattering. In Fig. 2(b), the photon statistics of the prolate- and oblate-based metamolecules are very similar irrespective of their different driving frequencies because the difference in their geometric factors is not sufficient to cause a noticeable change in $g^{(2)}(0)$.

Driving the metamolecule at the Fano peak leads to the emission of antibunched light ($g^{(2)}(0) < 1$) at short distances, $d \leq 4$ nm, which gradually transitions to coherent light ($g^{(2)}(0) \to 1$) at long distances, $d > 4$ nm (Fig. 2(b), red curves). At the Fano peak, driving the metamolecule at short distances leads to an antibunching effect as a result of constructive interference, i.e, the spontaneous emission of an absorbed incident photon is enhanced due to the Purcell effect [1,2]. The saturation of the metamolecule by a photon pair leads to a decrease in the two-photon scattering probability, $\langle (\mathscr{P}^-)^2 (\mathscr{P}^+)^2 \rangle$, at the Fano peak. As in the case of the dip, at the Fano peak, the transition from antibunched to coherent light at long distances is due to the vanishing Fano profile in Fig. 2(a).

4. Conclusion

We have shown that the driving frequencies (Fano peak, Fano dip, and plasmon peak), the MNP-QD distance, and the MNP geometry are all important factors to consider when designing metamolecules that exhibit different photon statistics. Our model shows that for a constant MNP volume, the choice of MNP geometry might affect the distance regimes where the metamolecule transitions from bunching to antibunching of the scattered photons, but not those where it transitions from antibunching to coherent emission. Fano interference makes it possible for the driven metamolecule to act as a saturable scatterer for photon statistics control.

Acknowledgments

The authors are grateful for the financial support from the South African Quantum Technology Initiative (SA QuTI), the department of science and innovation (DSI), and the national research foundation (NRF).

References

[1] Ridolfo A, Stefano O D, Fina N, Saija R and Savasta S 2010 *PRL* **105** 263601
[2] Waks E and Sridharan D 2010 *PRA* **82** 043845
[3] Zhao D, Gu Y, Chen H, Ren J, Zhang T and Gong Q 2015 *PRA* **92** 033836
[4] McEnery K R, Tame M S, Maier S A and Kim M S 2014 *PRA* **89** 013822
[5] Gisin N and Thew R 2007 *Nat. Photon.* **1** 165
[6] Lee C, Dieleman F, Lee J, Rockstuhl C, Maier S A and Tame M 2016 *ACS Photonics* **3** 992
[7] Wu X, Gray S K and Pelton M 2010 *Optics Express* **18** 23633
[8] Steck D A 2017 *Quantum and Atom Optics* (Available online at http://steck.us/teaching)
[9] Walls D F and Milburn G J 2008 *Quantum Optics, 2nd Edition* (Springer)
[10] Ugwuoke L C, Mančal T and Kruger T P J 2020 *JOSA B* **37**
[11] Johansson J R, Nation P D and Nori F 2013 *Comput. Phys. Commun.* **184** 1234